# Series Viscoelastic Actuators Can Match Human Force Perception

Federico Parietti, Gabriel Baud-Bovy, Elia Gatti, Robert Riener, Lino Guzzella, Heike Vallery

*Abstract*—Series Elastic Actuators (SEAs) have become frequently used for force control in haptic interaction, because they decouple actuator inertia from the end effector by a compliant element. This element is usually a metal spring or beam, where the static force-deformation relationship offers a cheap force sensor. For high-precision force control, however, the remaining small inertia of this elastic element and of the end effector still limit sensing performance and rendering transparency. Here, we extend the concept to deformable end effectors manufactured of viscoelastic materials. These materials offer the advantage of extremely low mass at high maximum deformation and applicable load. However, force and deformation are no longer statically related, and history of force and deformation has to be accounted for. We describe an observer-based solution, which allows drift-free force measurement with high accuracy and precision. Although the description of the viscoelastic behavior involves higher-order derivatives, the proposed observer does not require any numerical diffrention. This new integrated concept of sensing and actuation, called Series Viscoelastic Actuator (SVA), is applied to our high-precision haptic device OSVALD, which is targeted at perception experiments that require sensing and rendering of forces in the range of the human tactile threshold. User-device interaction force is controlled using state-of-the-art control strategies of SEAs. Force estimation and force control performance are evaluated experimentally and prove to be compatible with the intended applications, showing that SVAs open up new possibilities for the use of series compliance and damping in high-precision haptic interfaces.

*Index Terms*—Force measurement, force control, haptic interfaces, actuators, creep, elasticity

## I. INTRODUCTION

Haptic devices have been widely utilized for the study of human perception and sensorimotor control. Clinical applications are the assessment of neurological deficits [1], and robot-assisted rehabilitation [2]–[4]. Haptic devices help understand the mechanisms that underlie touch perception and identification [5]–[7].

Federico Parietti is with the Robotics Institute, Carnegie Mellon University, Pittsburgh, USA (fpariett@andrew.cmu.edu).

Gabriel Baud-Bovy is with the Department of Robotics, Brain and Cognitive Sciences, Istituto Italiano di Tecnologia, Genoa, Italy, and head of the Laboratory of Action, Perception and Cognition (LAPCO) at the San-Raffaele University of Milan, Italy (baud-bovy.gabriel@hsr.it).

Elia Gatti is with LAPCO at the San-Raffaele University of Milan, Italy (elia.gatti@kemart.it).

Robert Riener is head of the Sensory-Motor Systems Lab, Institute of Robotics and Intelligent Systems, ETH Zurich, Zurich, Switzerland, and Spinal Cord Injury Center, University Hospital Balgrist, Medical Faculty, University of Zurich (riener@mavt.ethz.ch).

Lino Guzzella is head of the Institute for Dynamic Systems and Control, Swiss Federal Institute of Technology (ETH), Zurich, Switzerland (lguzzella@ethz.ch).

Heike Vallery (corresponding author) is with the Sensory-Motor Systems Lab, Institute of Robotics and Intelligent Systems, ETH Zurich, Zurich, Switzerland, and Spinal Cord Injury Center, University Hospital Balgrist, Medical Faculty, University of Zurich (hvallery@ethz.ch, phone: +41 44 632 5316, fax: +41 44 632 1876).

| System | Max force | Static friction | User side inertia | Source |
|---|---|---|---|---|
| **Omega.3** | 12 N | 0.2 N* | >15 g† | spec., [5] |
| **Delta.3** | 20 N | 0.4 N* | >15 g | spec. |
| **Falcon** | 8.9 N | N/A | >15 g | spec. |
| **Phantom Omni** | 0.8 N | 0.26 N | 45 g | spec. |
| **Phantom Desk.** | 1.75 N | 0.06 N | 45 g | spec. |
| **Phantom P.1.0** | 1.4 N | 0.04 N | 75 g | spec. |
| **MIT Manus** | 45 N | <1.134 N | <1333 g | [14] |
| **Wristalyzer** | 6 Nm | N/A | 0.004 kgm$^2$ | [13] |

*: unpublished data. †: in combination with high-precision force sensor [5]

TABLE I
PERFORMANCE OF EXISTING HAPTIC SYSTEMS.

The application of haptic systems for such studies of human perception requires high accuracy in force measurement and control. Estimates of the human fingers' minimum force perception threshold range between 0.033 N [8] and 0.049 N [5], while the relative JND (just noticeable difference) for force is 7% of the stimulus magnitude [9]. The minimum force perception threshold sets the requirements for device sensing and control resolution. The recommended bandwidth for a haptic or teleoperation interface is 7 Hz [9], [10], because hand movements do not exceed 5-10 Hz. However, the human skin is capable of perceiving high-frequency vibrations (up to 1 kHz), which influences force perception.

To our knowledge, no haptic device is currently available that meets these specifications, although a variety of devices has been used in neurological research. The PHANToM [11] allows single-point interaction with virtual environments. Force Dimension's Omega and Delta are based on parallel kinematics, which can be expanded by passive and active end effectors. These systems possess 3D workspaces, but their linkages present multiple joints which introduce dry friction. The impedance-controlled planar robot MIT Manus [12] has been widely used in robot-aided therapy for stroke rehabilitation [3]. The Wristalyzer [13] is an admittance-controlled interface designed for wrist interaction, based on a traditional high-accuracy torque sensor. Both systems exhibit considerable end-effector inertia. Tab. I summarizes performance of current systems.

To overcome reflected inertia and allow high-precision force control, an alternative actuation principle is represented by Series Elastic Actuators (SEAs). SEAs decouple motor dynamics like friction and inertia, and they are inherently compliant. These advantages led to their application in rehabilitation robots [15], [16] and robotic manipulators [17]. The original SEA design consisted of a geared motor attached to a rotary or linear spring [18]. Also a modular series elastic element compatible with existing transmission components has been presented [19]. The SEA concept was later improved

with the introduction of a Bowden cable transmission, to mount the motor remotely [20], [21]. This allowed lighter joints, but introduced problems with friction and backlash. Hydraulic transmissions [22] solve this issue. However, for high-precision force applications, the mass of the deformable element itself and of the end effector is still an unsolved issue, which causes undesired dynamic effects.

Reflected inertia on the user side is the most critical requirement for our envisaged applications. To achieve this, we extend the SEA concept: The approach combines compliant functionality and end effector within one single deformable element. This maximizes rendering performance by minimizing undesired dynamic effects. The tight weight constraints are fulfilled by manufacturing the deformable end effector from thermoplastic material. The choice of a polymer requires an accurate model of its viscoelastic behavior [23]. This extends the principle of SEAs to Series Viscoelastic Actuators (SVAs). We show that the SVA, similarly to the SEA, allows accurate force measurement and control. In addition, the SVA can directly and transparently interact with the user, extending these benefits to the force range of human tactile perception. Introducing additional viscous properties to a SEA has been shown to be beneficial by Hurst et al. [24], who proposed to overcome bandwidth limitations of series elasticity by adding a parallel damper. In that context, damping was achieved by an additional element, and not by intrinsically combined material properties.

We show a first application of SVAs, which is a new haptic device to study human force perception. This device employs a series viscoelastic end effector to achieve high-accuracy force rendering at the fingertips of a human user who is constrained to move the hand at the wrist. Deformation is measured optically, so that no mass is added to the deforming part. The system is named OSVALD (Optical Series Viscoelastic Actuated Low-force Display). Particular emphasis is put on the mechanical optimization of the end effector and on the development of an algorithm to accurately estimate force from deformation, despite viscoelastic properties like creep and relaxation. This is achieved using an observer concept. Force measurement is compared to a high-precision piezoelectric sensor. The control scheme is based on conventional SEA control, which contains a force control loop cascaded with an inner velocity loop. Controller performance in terms of force tracking and bandwidth is experimentally evaluated and compared to theoretical expectations. The results show that the device is suitable for the intended investigations on human force perception.

## II. MECHANICAL DESIGN

The system has one rotational degree of freedom, interacting with the user about the wrist flexion/extension axis (Fig. 1). The system moves in the horizontal plane, avoiding gravitational effects. The end effector is a deformable beam with a spherical handle, held by the subject's fingertips in a pinch or key grasp. The distance $r$ of the handle from the wrist axis is adjustable (Fig. 2).

The main novel contribution is the use of an extremely lightweight series viscoelastic element as end effector. This
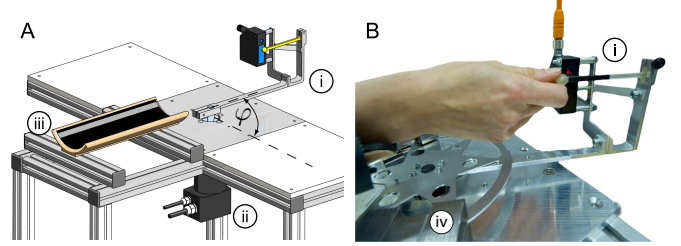


Fig. 1. OSVALD (Optical Series Viscoelastic Actuated Low-force Display). (**A**) Render showing the main components: (i) end-effector assembly with laser sensor and deformable thermoplast, (ii) direct-drive motor and (iii) arm brace. (**B**) Prototype, with (iv) eddy current damper.
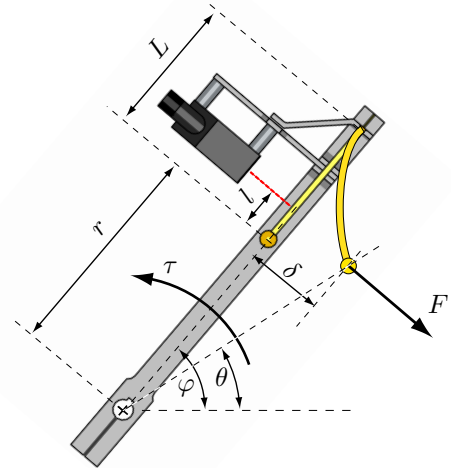


Fig. 2. Variables and sign conventions of OSVALD (top view). The user interacts through the tangential force $F$, which causes end-effector deflection $\delta$ (exaggerated in the figure). A laser sensor at position $l$ with respect to the handle measures this deflection. The radius $r$ is the distance between the wrist (aligned with the motor axis) to the end effector's spherical handle. The motor exerts a torque $\tau$, the lever angle is $\varphi$ (see Fig. 1). The user's wrist and fingers form a total angle of $\theta$ with the body's medio-lateral axis. As deflections are small, change of the radius $r$ is neglected.

combines the traditional advantages of SEAs with a particularly low endpoint mass: As in a SEA, the presence of series compliance decouples motor and lever inertia from the handle, and it increases inherent safety and robustness. In addition, bringing the viscoelastic element in direct contact with the subject's fingertips reduces endpoint mass to less than 1 g. The tight weight constraint led to a polymeric material. Good measurement resolution requires sufficient compliance, but maximum deformation must be limited, in order to keep the end effector movement tangential to the hand trajectory, and in order to allow rendering stiff environments [15]. Thus, its higher stiffness made a thermoplast preferable to an elastomer. We chose FullCure720, a rigid acrylic-based photopolymer (tensile strength 60.3 MPa, modulus of elasticity $E = 2.87$ GPa, elongation at break 20%, density 1092 kg/m$^3$), which is appropriate in terms of low weight, sufficient static stiffness and ability to inflect without permanent plastic deformation. At a maximum force of 3 N, the material deflects by 15 mm, causing an imperceptible 0.5% increase in the wrist-manipulandum distance $r$. The system operates at normal ambient temperature, thus far below the glassy transition value

of the polymer ($T_g = 48.7°C$). Rapid prototyping allows fine shape optimization, including a hollow cross section and a spherical handle. This simple design combines high force sensitivity with low manufacturing costs.

A crucial design choice concerns the measurement system used to determine end-effector deflection. Contact sensors must be excluded, since they would introduce undesired friction. Fiber-optic curvature sensors are light and adaptable, but they do not guarantee sufficient precision. Traditional strain gauges offer high precision but risk EM interference from the DC motor, and they require to be glued to the end effector, limiting its interchangeability. Fiber-optic strain gauges are immune to EM interference, but exceed the dimensions of the elastic element and pose tight limits on maximum deformation, which make them incompatible with the end effector's range of movement. Inductive and capacitive proximity sensors measure only limited distances, and the large-range types are too large and heavy for the lightweight end effector. Ultrasonic and infrared distance sensors present insufficient sampling rate and accuracy. An acceptable solution is offered by laser triangulation sensors, which can provide high resolution over a suitable range. The selected sensor offers acceptable precision at an affordable cost: resolution of 0.01 mm and sampling frequency of 1 kHz. Drawbacks of this choice are that the sensor is bulky and contributes 52 g to the lever mass.

The lever and motor were designed for low inertia and low Coulomb friction. We chose a maxon 400 W DC brushless motor with sinusoidal commutation for minimal torque ripple. The direct-drive design avoids friction and backlash, and the lightweight aluminum lever guarantees high stiffness and low inertia. The workspace is freely configurable within the interval of ±90°, which is suitable for both right- and left-handed subjects. An ergonomic brace supports the user's forearm.

Preliminary experiments showed that the device tends to resonate at high control gains. Therefore, an eddy current damper was added to introduce linear physical damping $\gamma$ without dry friction, as suggested in [25]. This element consists of a perforated disc with an effective annulus section of 10 mm and a total diameter of 80 mm (Fig. 1). Six C-shaped steel blocks hold permanent Neodym magnets (www.supermagnete.ch) inside, creating a magnetic field of strength 1 T in an air gap of 2.5 mm height. According to the recommendation of [26], the magnets overlap the annulus section. The disc is very thin (1.5 mm), so that its effective inertia is only 0.00014 kg m². In total, mass of the lever with all moving parts is 174 g, and inertia is 0.004 kg m².

The absence of a transmission requires a high-resolution quadrature encoder (8000 counts per turn). The device is controlled via Matlab xPC at a rate of 20 kHz. Encoder and drive support communication at this rate, the laser is oversampled accordingly.

## III. VISCOELASTIC FORCE SENSOR

### A. Viscoelastic Model

The thermoplastic end-effector material is not perfectly elastic, but governed by a constitutive equation that accounts for the history of loading and deformation [23]. Therefore, the assumption of Hooke's law would result in erroneous force predictions. Instead, the realization of an accurate force sensor based on end-effector deformation requires a detailed model of the material's viscoelastic behavior.

Linear viscoelastic theory [23], [27] provides a vast array of analog mechanical models to describe viscoelastic materials [28]. The two simplest schemes are the Maxwell model and the Voigt model. The former, constituted by a spring and a damper connected in series, responds to a constant strain with an exponentially decreasing stress (relaxation), and to a constant stress with an increasing permanent strain (creep). The latter, constituted by a spring and a damper connected in parallel, responds to a constant stress with a time-dependent strain, asymptotically converging to the pure elastic behavior (retarded elastic response); once the stress is removed, this model returns to its initial configuration without permanent strain (recovery). A viscoelastic material exhibits all of these behaviors. A serial combination of one Maxwell and one Voigt module, which is called Burgers model (Fig. 3), is the simplest
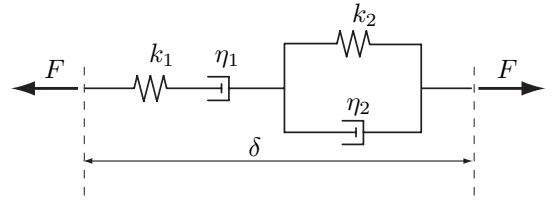


Fig. 3. The Burgers linear viscoelastic model describes end-effector dynamics. Parameters $k$ indicate elastic elements, while parameters $\eta$ indicate viscous elements. Spring and damper in series constitute a Maxwell block, while spring and damper in parallel constitute a Voigt block.

scheme to represent the force-deformation relationship of the thermoplastic end effector. Its constitutive equation is:

$$\ddot{F} + a\dot{F} + bF = c\ddot{\delta} + d\dot{\delta}, \tag{1}$$

where $\delta$ is the end effector deflection, and $F$ is the applied tangential force. The constant parameters

$$\begin{cases} a = (k_1 + k_2)/\eta_2 + k_1/\eta_1 \\ b = k_1 k_2/(\eta_1 \eta_2) \\ c = k_1/Q \\ d = k_1 k_2/(Q\eta_2) \end{cases} \tag{2}$$

contain the four Burgers model parameters $k_1$, $k_2$, $\eta_1$ and $\eta_2$ (Fig. 3): $k$ represents a stiffness and $\eta$ a damping coefficient, while the subscript 1 refers to the Maxwell module and 2 refers to the Voigt module. The geometric constant

$$Q = (l^3 + 3L^2 l + 2L^3)/(6I) \tag{3}$$

of the end-effector beam depends on its area moment of inertia $I$ and on the position $l$ of the laser sensor along the deformed beam of total length $L$ (Fig. 2). In purely elastic conditions, $F = c\delta = k_1/Q\delta$, with $k_1 = E$ the material's elastic module.

### B. Observer Design

Solving (1) for $\dot{F}$ and integrating yields

$$F = F(t_0) - \frac{1}{a}(\dot{F} - \dot{F}(t_0)) - \frac{b}{a}\int_{t_0}^{t} F \, \mathrm{d}\breve{t} + \frac{c}{a}\tilde{\dot{\delta}} + \frac{d}{a}\tilde{\delta}, \tag{4}$$

with variables transformed to omit initial conditions:

$$\tilde{\delta} := \delta - \delta(t_0), \quad \dot{\tilde{\delta}} := \dot{\delta} - \dot{\delta}(t_0) \tag{5}$$

The dependence of the force $F$ on the history of force and deflection generates the problem of drift in the force estimate. However, additional information is available to avoid such a drift: Knowledge on the "stiff" part (motor and lever) and history of the motor torque $\tau$ can be exploited, improving the estimate and suppressing a drift. The dynamics of this stiff part are

$$J\ddot{\varphi} = \tau - Fr - \gamma\dot{\varphi}. \tag{6}$$

Here, $J$ subsumes inertia of motor and lever about the motor axis of rotation. The radius $r$ is the distance between that axis and the end-effector handle (Fig. 2).

Combining dynamics of the stiff system (6) and the termoplast (4), the full system can be described in state-space form (See Appendix):

$$\begin{aligned} \dot{\boldsymbol{x}} &= \mathbf{A}\boldsymbol{x} + \mathbf{B}\boldsymbol{u} + \boldsymbol{w} \\ \boldsymbol{y} &= \mathbf{C}\boldsymbol{x} + \boldsymbol{v} \end{aligned} \tag{7}$$

The state vector $\boldsymbol{x}$ is chosen as

$$\boldsymbol{x} = \begin{bmatrix} \int_{t_0}^t F\mathrm{d}\breve{t} - \frac{1}{b}\dot{F}(t_0) - \frac{a}{b}F(t_0) & F - c\tilde{\delta} & \varphi & \dot{\varphi} \end{bmatrix}^T, \tag{8}$$

and input $\boldsymbol{u}$ and output $\boldsymbol{y}$ are

$$\boldsymbol{u} = \begin{bmatrix} \tilde{\delta} & \tau \end{bmatrix}^T, \quad \boldsymbol{y} = \begin{bmatrix} \varphi & \dot{\varphi} \end{bmatrix}^T. \tag{9}$$

The second component of $\boldsymbol{x}$ has been chosen such that the derivative $\dot{\tilde{\delta}}$ of the laser sensor measurement is not needed as input for the observer.

The process noise vector $\boldsymbol{w}$ accounts for dry friction in the bearings and for sensor noise on the deflection measurement $\delta$. Process noise $\boldsymbol{v}$ describes noise on the encoder and its derivative. The system (7) is observable. The covariance matrices of the noise vectors $\boldsymbol{w}$ and $\boldsymbol{v}$ are used to design a Kalman filter, to obtain stochastically optimal estimates $\hat{\boldsymbol{x}}$ of the state vector $\boldsymbol{x}$.

To obtain the force estimate $\hat{F}$, the elastic component $c\tilde{\delta}$ from the laser sensor measurement is added to the second observer state estimate:

$$\hat{F} = \begin{pmatrix} 0 & 1 & 0 & 0 \end{pmatrix} \hat{\boldsymbol{x}} + c\tilde{\delta}. \tag{10}$$

This means that dynamic forces, captured by the laser as instantaneous elastic deformations, are incorporated in the estimate without delay; viscous material properties are accounted for by the state equations.

It should be noted that the second output in $\boldsymbol{y}$, motor speed, is not necessary to make (7) observable. Nevertheless, the filtered derivative of $\varphi$ is used here as an additional input to the Kalman filter. The practical reason is that $\varphi$ can be obtained at the 20 kHz encoder sampling rate, whereas the observer input $\tilde{\delta}$ depends on the 1 kHz information of the laser sensor.

## C. Parameter Identification

After integration, the description of the viscoelastic end effector (4) does not include derivatives of order higher than the first. Furthermore, it is linear in the substitute parameters $1/a, b/a, c/a$, and $d/a$. This allows simple identification using Least-Squares regression, minimizing the squared error between $F$ obtained from (4) and $F$ measured by a high-precision force sensor over a given time interval. In order to provide reference force measurements, a Kistler 9205 piezoelectric sensor is employed (precision: 0.0005 N). Due to its own mass and inertia, the piezoelectric force sensor can only provide accurate measurements when it does not move. Therefore, it is rigidly mounted within an experimental setup (Fig. 4), and it is connected to the end effector using light-weight fishing line. This Nylon line also exhibits viscoelastic behavior. However, it is important to note that any elastic deformation or creep of the line does not influence the measurement, because force on both ends is still identical. The deformation should only not be so large that it noticeably changes the angle of attack of the line at the handle. To generate forces, the electric motor is used in different experimental conditions. It imposes forces of different amplitudes (0-1.5 N) and frequencies (0-15 Hz) on the end effector, with patterns including sinusoidal oscillations in the target frequency band, multiple steps, and ramps. End-
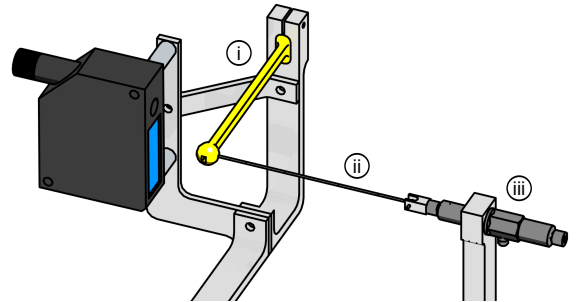


Fig. 4. Experimental setup for viscoelastic model identification. The end effector is rigidly mounted on the revolving lever (i), which also supports the laser sensor. A Nylon line (ii) connects the end-effector handle to the high-precision piezoelectric force sensor (iii), which is fixed to a rigid support.

effector deformation $\delta$ is obtained from the laser. The first-order derivatives of force and deflection in (4) are computed off-line using filtered differentiation with zero phase lag (2nd-order Butterworth filter applied backward and forward, 50 Hz cutoff frequency). Using the full set of data, the identified model parameters are: $k_1 = 2.87$ GPa, $k_2 = 11.68$ GPa, $\eta_1 = 737$ Gpa s, $\eta_2 = 0.57$ GPa s.

In order to identify the stiff part, multiple experiments are performed for subsequent regression. First, the Kistler sensor is used to determine gain and offset of the motor-drive unit. For this, we used very slow (to avoid inertial effects) and symmetric (to cancel influence of friction) movements. The gain was close to the specifications (5.4% lower). Friction and inertia were identified by separate experiments, where the motor tracked a reference angle, and no force acted on the handle. For friction, the motor tracked a slowly varying pseudorandom reference angle. From this measurement, dry

and viscous friction in the motor bearings, as well as damping of the magnetic brake were identified using regression. Maximum dry friction was equivalent to 0.11 N endeffector force, and viscous damping $\gamma/r^2$ to 5.9 Ns/m with damper, and 0.45 Ns/m without damper. To identify inertia, the motor tracked a multisine reference angle with increasing frequency, the resulting value was $J = 0.0103\,\mathrm{kgm}^2$.

Noise covariance matrices for the Kalman filter were chosen as diagonal matrices, assuming independence of errors in $\boldsymbol{v}$ and $\boldsymbol{w}$. Standard deviations were assumed from encoder resolution ($7.9 \cdot 10^{-4}$ rad), laser quantization (0.01 mm) and dry friction in the motor bearings.

## IV. FORCE CONTROL OF THE SVA

Apart from the observer the SVA needs for hidden states, the controller structure is similar to that of SEAs. The first SEA prototypes used PID force control combined with feedforward terms [18]. This scheme had its main drawbacks in the limited robustness to friction and backlash. Later, an impedance controller was coupled with an inner position loop [20]. Finally, a cascaded force control with fast inner motor velocity loop [19], [29] was proposed, which is advantageous in terms of stability and performance [15], [30].

We use such a cascaded force-velocity scheme, but without integration in the inner loop. The integrator is not necessary in theory, and it negatively affected controller performance in practice. Therefore, the motor torque $\tau$ is:

$$\tau = r[F_{\mathrm{ref}} + P_V(r\dot{\varphi}_{\mathrm{ref}} - r\dot{\varphi})] \text{ , with} \quad (11)$$

$$r\dot{\varphi}_{\mathrm{ref}} = P_F(F_{\mathrm{ref}} - F) + I_F \int (F_{\mathrm{ref}} - F)\mathrm{d}t \quad (12)$$

The reference torque $F_{\mathrm{ref}}$ could emulate a variety of virtual environments - e.g. springs, dampers, or free motion. This reference torque is used as a feed-forward term for the motor, and as a reference for a proportional-integral force controller with proportional gain $P_F$ and integral gain $I_F$. The controller output is used as a reference for a fast inner velocity loop with proportional gain $P_V$. The outer loop is restricted by the sampling rate of the laser sensor (1 kHz), but the inner loop can exploit the fast response of the drive (20 kHz).

The observer provides estimates both for force $F$ and for lever angular velocity $\dot{\varphi}$ to be used in this control scheme. This means that no numerical differentiation is necessary, neither for observer nor for controller implementation.

Control gains are chosen such that the theoretical impedance frequency response has a phase that stays within the bounds of -90 to 90°, as a necessary condition for passivity [31]. Chosen gains are: $P_V = 6$ Ns/m, $P_F = 2$ m/(Ns), $I_F = 10$ m/(Ns$^2$).

## V. TECHNICAL PERFORMANCE ANALYSIS

### A. Error Sources

Measurement error is a superposition of various components: Laser resolution leads to a quantization of 0.0033 N, limiting dynamic precision. Viscoelastic behavior can cause a drift, limiting static accuracy. The observer compensates for this slow drift, but it relies on motor current as input. Thus, the measurement can still drift within the range of motor dry

friction. This friction is generated in the bearings, as the motor itself is brushless. Viscous friction is not problematic, as it is incorporated in the observer model. Another error source is end effector inertia. As the mass is below 1 g, this error is expected to be below the human perception threshold.

Force control performance varies with frequency: The general benefit of a SEA is that the compliant element hides inertia of any preceding structure (here motor and lever assembly). For high frequencies, a stiff device exhibits an asymptotic frequency response behavior of a pure mass. In a SEA, intrinsic spring dynamics define the asymptotic behavior instead. In an intermediate frequency range, reflected behavior is that of a damper. Its damping constant $k_D$ depends on control gains: $k_D = P_V/(P_V P_F + 1)$ [15]. With the control gains given above, the reflected damping for OSVALD would theoretically be $k_D$=0.46 Ns/m. High control gains and intrinsic compliance also prevent friction in the bearings to be felt by the user. End-effector dynamics, however, cannot be compensated. In OSVALD, the extremely small end-effector mass and the optical measurement principle make uncompensated inertia and friction negligible.

### B. Experimental Setup and Protocol

The observer-based force sensing is evaluated on a leave-one-out basis, using the same set of calibration data as used for parameter identification in Sec. III-C: The parameters are identified based on all the datasets except for one, then they are used to estimate the force for the omitted data set. To evaluate force sensing performance of the SVA, the observed force is compared to the piezoelectric sensor measurements. As the Kistler force sensor is mounted rigidly, its inertia does not influence the measurements. However, this is not a "static" condition, because the lever moves while the thermoplast deforms in the opposite direction.

To evaluate force control performance, both a force-tracking experiment and a zero-force experiment are conducted. For force tracking, the end effector is manually restrained while the device is given a reference sinusoidal force that varies both in amplitude and frequency: Frequency slowly increases from 2 to 15 Hz, with multiple oscillations for each frequency, while amplitude of force $F$ decreases from 0.5 to 0.07 N. The expected force value at the end effector is compared to the one estimated by the state observer in terms of phase lag and amplification in steady state for each frequency. The experiment is done with and without the eddy current damper, to separately assess the influence of this element. For zero-force performance, the handle is manually excited with varying frequencies, and the frequency response is estimated using spectral analysis [32].

### C. Results

Fig. 5 shows the results that were obtained with the measurement setup of Fig. 4 and experimental conditions described in Sec. V-B. A simple elastic model, which does not take into account creep and relaxation, drifts considerably compared to the piezoelectric sensor; the RMS error over all data sets reaches 0.22 N with such a purely elastic model. The observer,
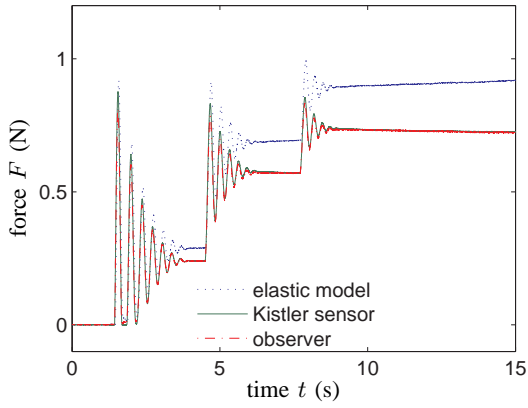
Fig. 5. Comparison between a purely elastic model and the observer output. The correct force is measured by a high-precision piezoelectric sensor.

which is based on the viscoelastic model and on dynamics of the motor-lever system, reduces this estimation error: The resulting mean error over all data sets is limited to 0.048 N.

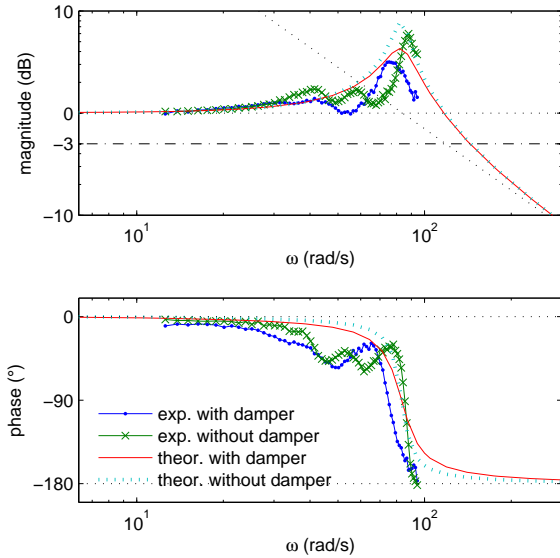Theoretical and experimental frequency responses for force tracking are shown in Fig. 6, with and without eddy current damper. The bandwidth of the device is about 16 Hz.



Fig. 6. Theoretical and experimental tracking frequency response of the SVA with theoretical asymptotes, with and without eddy-current damper. The markers indicate the frequencies where the steady-state response was evaluated.

The impedance transfer function relates translational speed $r\dot{\theta}$ of the fingertips to the opposing force $F$ generated by the device (Fig. 7). As expected, impedance asymptotically approaches zero for low and for high frequencies. For an intermediate frequency range, apparent dynamics are bounded by a damper behavior, as stated in V-A. The eddy current damper lowers this bound, such that the resulting equivalent forces perceived by the user are always smaller than those generated by a damper with damping constant 1.34 N/(m/s).

One adverse effect was observed when the handle is held

still in zero-force control. Under these conditions, high-frequency ($\approx$11 Hz) and low-amplitude ($\approx$.02 N) oscillations are sometimes perceivable, depending also on the firmness of the fingers' grip.
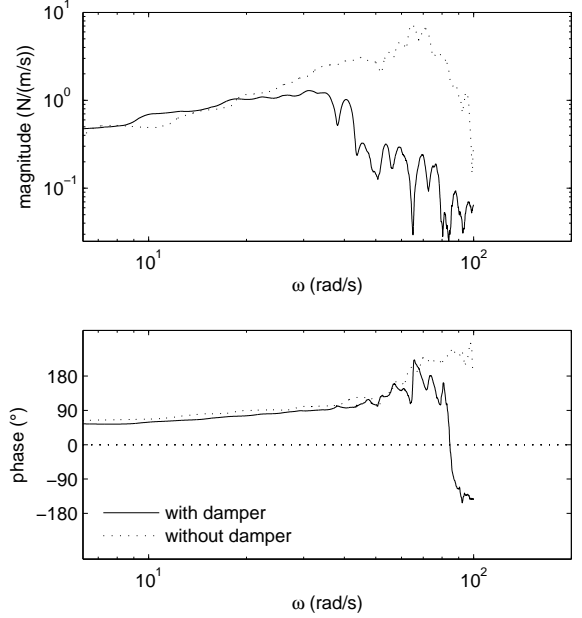


Fig. 7. Empirical impedance frequency response of the SVA in zero-force control, with and without eddy-current damper.

### D. Discussion

The viscoelastic model is both accurate in its force predictions and consistent with theoretical parameters. In the Burgers model, the elasticity $k_1$ is equivalent to the glassy material elasticity, and the identified parameter corresponds (0.03% smaller) to the specified material's $E$ modulus.

Force rendering performance fulfills the requirements, as apparent dynamics are bounded by damper behavior: The required force of 0.03 N is not exceeded for movement speeds below 20 mm/s. Bandwidth requirements of 10 Hz are also met.

A reason for the adverse high-frequency oscillations in zero-force control could be undesired elasticity in the lever or the bulky laser assembly, so system performance could potentially be improved by a better distance sensor. The introduction of the physical eddy-current damper already reduced resonance. Encouraged by these findings, we modified the damper to have 36 permanent magnets and the disc to have a larger annulus section. This allowed us to increase force gains to $P_F = 5$ m/(Ns), $I_F = 15$ m/(Ns$^2$), $P_V = 8$ Ns/m, and it solved the problem of small oscillations. We used this modified setup for the experiments described in the next section.

The viscoelastic model identification has only been performed at ambient temperature and pressure. Effects connected to the variation of these factors have not been considered.

Like a SEA, the SVA is particularly useful to render low impedances, and less to render stiff environments. Furthermore, rendering objects with inertia would be difficult.

## VI. Psychophysical Experiment

We conducted a first psychophyiscal experiment to measure the absolute force direction identification threshold, which is the minimum force necessary to identify the direction of a weak force ($<0.2\,$N). This experiment requires OSVALD to render forces very accurately.

### A. Setup and Protocol

Twelve healthy subjects participated in the experiment (3 female, mean age 29). At the beginning of the experiment, the participants sat comfortably in front of the device, resting their right forearm on the support and grasping the handle between thumb and index with a key grasp (Fig. 1 B).

After a brief familiarization period, the participants closed their eyes for the entire duration of the experiment (about 45 minutes with a short pause in the middle). At the beginning of each trial, participants actively moved the hand to the initial position, arrival was indicated by a beep. After the beep, the device produced a force that increased linearly with time over a 3.5 s period until it reached the target level. A second beep with different pitch indicated the end of this loading phase. The participants were asked to keep their arm and hand immobile after the first beep and to indicate the perceived direction of the force ("left" or "right") after the second beep. The stimuli for the first four subjects consisted of a force of 0, 0.03, 0.07, 0.12, or 0.18 N in one of the two possible directions. The stimuli for the last seven subjects consisted of a force of 0, 0.01, 0.03, 0.07, or 0.12 N. The experiment comprised ten blocks of ten trials each. The order of presentation of the ten stimuli (4 force levels times 2 directions plus 2 times 0 N force) was randomized within each block.

To compute the force threshold, we fitted a logistic psychometric function to the percentage of correct responses as a function of the (non-null) force magnitude for each subject. The range of the psychometric function was fixed between 0.5 (chance level) and 1. The force direction identification threshold was defined as the force magnitude that yielded 75% of correct responses (Fig. 8). For the trials with zero force, we computed the percentage of responses indicating a rightward force (see [5] for more details on data analysis).

As a quality check, we recorded the force produced by the device during 32 intervals of 25 s duration each, randomly selected over the entire course of the experiment (sampling rate 20 kHz). The intervals covered trials performed by different participants and periods during which the device rendered different force levels. In order to compute the RMS force error in static and in dynamic conditions, we separated time intervals depending on the subjects' movement speed. Speed was calculated by off-line numerical differentiation of the position signal, after applying a second-order Butterworth filter (cutoff 10 Hz and a cubic smoothing spline (smoothing parameter =0.5). Below a threshold of 5 mm/s for absolute speed, we defined the arm as immobile.

### B. Results

We could not compute the threshold for one subject because performance was always above the threshold even with the
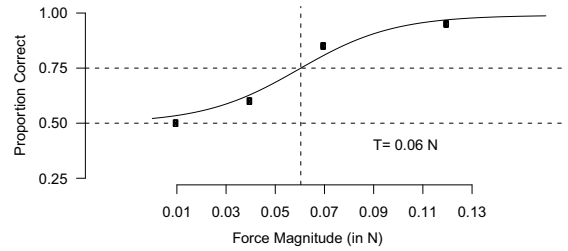


Fig. 8. Threshold determination for a representative participant: A psychometric function fitted to the proportion of correct responses as a function of stimulus intensity. The threshold $T=0.06\,$N corresponds to 75% of correct responses.

smallest stimulus (0.03 N) and for another subject because response seemed random and performance never reached the threshold. The average ($\pm$SD) thresholds for the remaining ten participants were $0.056\pm0.011\,$N. To examine a potential response bias, we computed the number of responses left or right when no force was delivered to the subjects. Only one subject had a preference for one of the two responses outside the 90% binomial interval of confidence around the chance level, which might indicate a response bias.

When the subjects kept their arm immobile (51.5% of the samples collected), the RMS force error was 0.018 N. During movements, error increased, as expected (RMS=0.023 N).

### C. Discussion

The average threshold of about 6 g is in line with the results found in [5]. Differences between the two studies are probably due to the differences in experimental setting and in the subjects' grasping behavior. For example, in the present experiment, the force acted primarily on the digits and wrist joint since the arm was supported by a brace. Moreover, it is possible that participants grasped the OSVALD handle with less force than in [5]. In this case, the mechanoreceptors in the skin would be stimulated more, because greater compliance of the fingerpad with small grip force [33] allows a bigger stretch of the skin in tangential direction. Finally, a smaller grip force will also decrease the activation due to the normal force, which is likely to mask information about the tangential force. Future work on the OSVALD device will consider the possibility of measuring the grip force on the handle. The low threshold measured in the experiment clearly demonstrates the need for an accurate force rendering device.

## VII. Conclusion

Series viscoelastic elements as deformable end effectors, in combination with observer-based force estimation, allow the realization of high-accuracy force sensing and control. This integrated sensing and actuation principle, the Series Viscoelastic Actuator (SVA), enables haptic interaction in the force range of the human sensory threshold.

## REFERENCES

[1] D. Meary, G. Baud-Bovy, R. Chieffo, L. Leocani, M. Comola, and G. Comi, "Robot-assisted assessment of sensorimotor control: A case study," in *Proc. IEEE Int. Workshop Medical Measurements and Applications (MeMeA)*, 2009, pp. 172–176.

[2] O. Lambercy, L. Dovat, H. Yun, S. K. Wee, C. Kuah, K. Chua, R. Gassert, T. Milner, C. L. Teo, and E. Burdet, "Rehabilitation of grasping and forearm pronation/supination with the haptic knob," in *Proc. IEEE Int. Conf. Rehabilitation Robotics (ICORR)*, 2009, pp. 22–27.

[3] G. B. Prange, M. J. A. Jannink, C. G. M. Groothuis-Oudshoorn, H. J. Hermens, and M. J. Ijzerman, "Systematic review of the effect of robot-aided therapy on recovery of the hemiparetic arm after stroke." *J Rehabil Res Dev*, vol. 43, no. 2, pp. 171–184, 2006.

[4] M. Ferraro, J. J. Palazzolo, J. Krol, H. I. Krebs, N. Hogan, and B. T. Volpe, "Robot-aided sensorimotor arm training improves outcome in patients with chronic stroke." *Neurology*, vol. 61, no. 11, pp. 1604–1607, Dec 2003.

[5] G. Baud-Bovy and E. Gatti, "Hand-held object force direction identification thresholds at rest and during movement," in *EuroHaptics*, 2010, pp. 231–236.

[6] G. Robles-De-La-Torre and V. Hayward, "Force can overcome object geometry in the perception of shape through active touch." *Nature*, vol. 412, no. 6845, pp. 445–448, Jul 2001.

[7] L. Dominjon, A. Lecuyer, J.-M. Burkhardt, P. Richard, and S. Richir, "Influence of control/display ratio on the perception of mass of manipulated objects in virtual environments," in *Proceedings of IEEE Virtual Reality (VR)*, 2005, pp. 19–25.

[8] H. H. King, R. Donlin, and B. Hannaford, "Perceptual thresholds for single vs. multi-finger haptic interaction," in *Proc. IEEE Haptics Symp*, 2010, pp. 95–99.

[9] H. Tan, J. Radcliffe, B. No, H. Z. Tan, B. Eberman, M. A. Srinivasan, and B. Cheng. (1994) Human factors for the design of force-reflecting haptic interfaces.

[10] T. Brooks, "Telerobotic response requirements," in *Proceedings of the IEEE International Conference on Systems, Man and Cybernetics*, nov. 1990, pp. 113 –120.

[11] *PHANToM haptic interface: a device for probing virtual objects*, ser. Proceedings of the 1994 International Mechanical Engineering Congress and Exposition, vol. 55-1. Massachusetts Inst of Technology, Cambridge, United States: ASME, 1994.

[12] N. Hogan, H. I. Krebs, J. Charnnarong, P. Srikrishna, and A. Sharon, "Mit-manus: a workstation for manual therapy and training. i," in *Proc. Workshop IEEE Int Robot and Human Communication*, 1992, pp. 161–165.

[13] G. Grimaldi, P. Lammertse, N. Braber, J. Meuleman, and M. Manto, "A new myohaptic device to assess wrist function in the lab and in the clinic — the wristalyzer," in *Proceedings of the 6th international conference on Haptics: Perception, Devices and Scenarios*, ser. EuroHaptics '08. Berlin, Heidelberg: Springer-Verlag, 2008, pp. 33–42.

[14] H. Krebs, M. Ferraro, S. Buerger, M. Newbery, A. Makiyama, M. Sandmann, D. Lynch, B. Volpe, and N. Hogan, "Rehabilitation robotics: pilot trial of a spatial extension for mit-manus," *Journal of NeuroEngineering and Rehabilitation*, vol. 1, no. 1, p. 5, 2004.

[15] H. Vallery, J. Veneman, E. van Asseldonk, R. Ekkelenkamp, M. Buss, and H. van Der Kooij, "Compliant actuation of rehabilitation robots," *IEEE Robotics & Automation Magazine*, vol. 15, no. 3, pp. 60–69, 2008.

[16] K. Kong, J. Bae, and M. Tomizuka, "A compact rotary series elastic actuator for human assistive systems," *IEEE/ASME Transactions on Mechatronics*, vol. PP, no. 99, pp. 1 –10, 2011.

[17] H. Seki, Y. Kamiya, and M. Hikizu, "SCARA Type Robot Arm with Mechanically Adjustable Compliant Joints," in *Proceedings of the IEEE Conference on Emerging Technologies and Factory Automation (ETFA)*, Sep. 20–22, 2006, pp. 1175–1181.

[18] G. A. Pratt and M. M. Williamson, "Series elastic actuators," in *Proc. IEEE/RSJ Int Intelligent Robots and Systems 95. 'Human Robot Interaction and Cooperative Robots' Conf*, vol. 1, 1995, pp. 399–406.

[19] G. Wyeth, "Control issues for velocity sourced series elastic actuators," in *In Proceedings of Australasian Conference on Robotics and Automation*, 2006.

[20] G. A. Pratt, P. Willisson, C. Bolton, and A. Hofman, "Late motor processing in low-impedance robots: impedance control of series-elastic actuators," in *Proc. American Control Conf the 2004*, vol. 4, 2004, pp. 3245–3251.

[21] J. F. Veneman, R. Ekkelenkamp, R. Kruidhof, V. D. Helm, and H. van der Kooij, "A series elastic- and bowden-cable-based actuation system for use as torque actuator in exoskeleton-type robots," *Int. J. Robot. Res.*, vol. 25, no. 3, pp. 261–281, March 2006.

[22] A. Stienen, E. Hekman, H. ter Braak, A. Aalsma, F. van der Helm, and H. van der Kooij, "Design of a rotational hydroelastic actuator for a powered exoskeleton for upper limb rehabilitation," *IEEE Transactions on Biomedical Engineering*, vol. 57, no. 3, pp. 728 –735, 2010.

[23] W. G. Knauss, I. Emri, and H. Lu, "Mechanics of polymers: Viscoelasticity," in *Springer Handbook of Experimental Solid Mechanics*, W. N. Sharpe, Ed. Springer US, 2008, pp. 49–96.

[24] J. Hurst, D. Hobbelen, and A. Rizzi, "Series Elastic Actuation: Potential and Pitfalls," in *Proceedings of the International Conference on Climbing and Walking Robots*, 2004.

[25] J. E. Colgate and J. M. Brown, "Factors Affecting the Z-Width of a Haptic Display," in *Proceedings of the IEEE International Conference on Robotics & Automation (ICRA)*, San Diego, CA, 1994, pp. 3205–10.

[26] A. Gosline and V. Hayward, "Eddy Current Brakes for Haptic Interfaces: Design, Identification, and Control," *IEEE/ASME Transactions on Mechatronics*, vol. 13, no. 6, pp. 669 –677, 2008.

[27] W. Kaiser, W. N. Findley, J. S. Lai, and K. Onaran, "Creep and relaxation of nonlinear viscoelastic materials with an introduction to linear viscoelasticity," *Z. angew. Math. Mech.*, vol. 58, no. 11, pp. 524–524, 1976.

[28] D. Roylance, "Engineering viscoelasticity," 2001, cambridge, MA: MIT Press.

[29] J. W. Sensinger and R. F. ff. Weir, "Improvements to series elastic actuators," in *Proceedings of the 2nd IEEE/ASME International Conference on Mechatronic and Embedded Systems and Applications*, 2006, pp. 1 –7.

[30] H. Vallery, R. Ekkelenkamp, H. van der Kooij, and M. Buss, "Passive and accurate torque control of series elastic actuators," in *Proc. IEEE/RSJ Int. Conf. Intelligent Robots and Systems (IROS)*, 2007, pp. 3534–3538.

[31] J. E. Colgate, "The Control of Dynamically Interacting Systems," Ph.D. dissertation, MIT Department of Mechanical Engineering, 1988.

[32] L. Ljung, *System identification: Theory for the user*, 2nd ed. prentice hall, 1999.

[33] V. Hayward, O. Astley, M. Cruz-Hernandez, G. D., and G. Robles-De-La-Torre, "Haptic interfaces and devices sensor review," *ProQuest Science Journal*, vol. 24, no. 1, 2004.

## APPENDIX

Combining (4) and (6), the matrices of the state-space system (7) are:

$$\mathbf{A} = \begin{bmatrix} 0 & 1 & 0 & 0 \\ -b & -a & 0 & 0 \\ 0 & 0 & 0 & 1 \\ 0 & -r/J & 0 & -\gamma/J \end{bmatrix} \quad (13)$$

$$\mathbf{B} = \begin{bmatrix} c & 0 \\ d-ac & 0 \\ 0 & 0 \\ -rc/J & 1/J \end{bmatrix}, \mathbf{C} = \begin{bmatrix} 0 & 0 & 1 & 0 \\ 0 & 0 & 0 & 1 \end{bmatrix} \quad (14)$$

As the eddy-current damper was added at a later stage, observer evaluation had been done with $\gamma = 0$.